Princeton Plasma Physics Laboratory

PPPL-5132

The Tokamak Density Limit: a Thermo-resistive Disruption Mechanism

D. A. Gates, D. P. Brennan, L. Delgado-Aparicio, R. B. White

July 2015

Prepared for the U.S. Department of Energy under Contract DE-AC02-09CH11466.

Princeton Plasma Physics Laboratory
Report Disclaimers

Full Legal Disclaimer

Trademark Disclaimer

PPPL Report Availability

Princeton Plasma Physics Laboratory:

http://www.pppl.gov/techreports.cfm

Office of Scientific and Technical Information (OSTI):

http://www.osti.gov/scitech/

Related Links:

U.S. Department of Energy

U.S. Department of Energy Office of Science

U.S. Department of Energy Office of Fusion Energy Sciences

PPPL-5132

The Tokamak Density Limit: a Thermo-resistive Disruption Mechanism*

D. A. Gates, D. P. Brennan, L. Delgado-Aparicio, R. B. White

Plasma Physics Laboratory, Princeton University, P.O.Box 451, Princeton, New Jersey 08543

Abstract

The behavior of magnetic islands with 3D electron temperature and the corresponding 3D resistivity effects on growth are examined for islands with near-zero net heating in the island interior. We refer to this class of non-linearities as thermo-resistive effects. In particular the effects of varying impurity mix on the previously proposed local island onset threshold [Gates and Delgado-Aparicio, PRL 2012] are examined and shown to be consistent with the well established experimental scalings for tokamaks at the density limit. A surprisingly simple semi-analytic theory is developed which imposes the effects of heating/cooling in the island interior as well as the effects of island geometry. For the class of current profiles considered it is found that a new term that accounts for the thermal effects of island asymmetry is required in the Modified Rutherford Equation. The resultant model is shown to exhibit a robust onset of a rapidly growing tearing

mode - consistent with the disruption mechanism observed at the density limit in tokamaks. A fully non-linear 3D cylindrical calculation is performed that simulates the effect of net island heating/cooling by raising/suppressing the temperature in the core of the island. In both the analytic theory and the numerical simulation the sudden threshold for rapid growth is found to be due to an interaction between three distinct thermal non-linearities which affect the island resistivity, thereby modifying the growth dynamics.

It has been shown that an approximate criterion for the internal power balance in a magnetic island, when combined with a simple model for the current profile [1], is qualitatively and semi-quantitatively consistent with the empirical density limit scaling for tokamaks known as the Greenwald limit [2, 3]. It has also been shown in Reference [4] that the current profiles corresponding to the density limit which were found in reference [1] generate small saturated islands at the $q = 2$ surface if only the classical Δ' is used as a drive term in the modified Rutherford equation [5, 6]. In this paper we discuss several important aspects of the behavior of tearing modes near the density limit in tokamaks, including relevant new physics effects in this important regime.

We now examine the effect of impurity mixture on the density limit. Various collisional processes contribute to the plasma cooling or the total power loss by radiation, which has to be balanced by the Ohmic heating power in the island interior. These processes can be due to, a) a continuous radiation spectrum resulting from Bremsstrahlung due to electron-ion collisions (free-free) and recombination (free-bound), b) line-radiation from hydrogen or deuterium as well as intrinsic and extrinsic impurities, and c) cyclotron radiation, which could lead to substantial power loss but is immediately re-absorbed since the plasma is often optically thick at the fundamental frequency. The most important source for radiative power losses are thus impurity ions, which produce both Bremsstrahlung and line radiation emission.

A relatively simple model for the local radiated power density (P^V_{rad}) is found by using hydrogenic Bremsstrahlung for the deuterium contribution and a temperature-dependent steady-state radiative cooling rate summed over all impurity species, such that, $P^V_{rad} = n_e n_D L_D(T_e) + \sum n_e n_Z L_Z(T_e)$. The onset criteria for radiation driven tearing modes can be quantified using electron power balance between the local Ohmic heating and the radiated power density as,

$$\frac{m_e}{e^2}\frac{Z_{eff}}{(\tau_{e,D} n_D)} J^2 > n_e^2 L_D \hat{P}^V_{rad} \tag{1}$$

where, $\tau_{e,D} n_D$ is the electron-deuterium collision time and the deuterium density, J is the Ohmic current density, and $\hat{P}^V_{rad} \equiv P^V_{rad}/n_e^2 L_D$ is a dimensionless figure of merit defined as a radiative power density normalized to that of the Bremsstrahlung losses in a pure plasma. The quantity L_D is the effective cooling rate as defined in reference [7]. Equation 1 can be reduced to a functional form shown in Equation 3. This equation relates the local maximum achievable density at the rational surface and resembles that of the maximum average plasma density given by the well known Greenwald density limit also shown below.

$$n_e[\times 10^{20}\mathrm{m}^{-3}] < \mathcal{F}_{D,Z} \cdot J \left[\frac{\mathrm{MA}}{\mathrm{m}^2}\right] \tag{2}$$

$$\bar{n}_e[\times 10^{20}\mathrm{m}^{-3}] < n_G \equiv \frac{I_p[\mathrm{MA}]}{\pi a^2[\mathrm{m}^2]} \tag{3}$$

The function $\mathcal{F}_{D,Z}$ includes all the local information pertinent to both plasma and atomic physics, namely the values of the effective charge, Coulomb-logarithm, plasma temperature and the normalized radiated power density,

$$\mathcal{F}_{D,Z} \approx \sqrt{\frac{0.61 \cdot Z_{eff} \cdot \ln \Lambda_{e,D}}{T_e^2[\mathrm{keV}] \cdot \hat{P}^V_{rad}}}. \tag{4}$$

Hereafter we will consider a plasma with two impurities, Carbon and Iron. The carbon and iron mix represents a simple, yet reasonably realistic

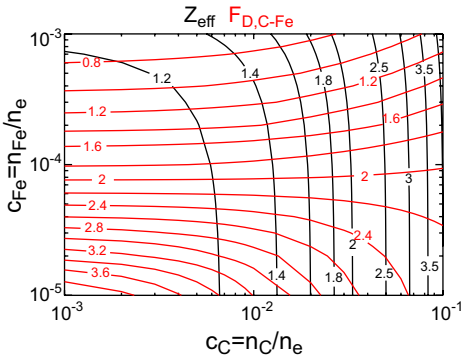

Figure 1: Contours of Z_{eff} and $\mathcal{F}_{D,Z}$ as a function of carbon and iron concentrations for an electron temperature of 500eV.

scenario of low-Z plasma facing components and high-Z impurities sputtering off the containment wall. Contours of Z_{eff} and $\mathcal{F}_{D,C-Fe}$ are plotted in Figure 1 for a plasma temperature of 500eV and a wide range of carbon and iron concentrations from 10^{-3} to 10^{-1} and 10^{-5} to 10^{-3}, respectively. Nearly unmeasurable changes in Z_{eff} introduced by a high-Z metallic contribution can be responsible for substantially altering the power balance. For instance, along a constant contour of $Z_{eff} = 1.5$ - generally measured in tokamak and reverse field pinch devices, the local radiated power density can increase by nearly two orders of magnitude thus limiting the maximum achievable density.

The density limit function $\mathcal{F}_{D,C-Fe}$ depicted in 1 shows a strong depen-

dence on the concentration of high-Z impurities and is nearly unaffected by the carbon concentration. A scan of two-orders of magnitude of $c_C = n_C/n_e$ at a fixed $c_{Fe} = n_{Fe}/n_e = 8 - 10 \times 10^{-5}$ yields the same $\mathcal{F}_{D,C-Fe} \approx 2.0$. However, at a fixed carbon concentration of 1% the density limit could be easily reduced by a factor of two when the iron concentration reaches 10^{-4} without any noticeable change in Z_{eff}. Figure 2 should be compared to Figure 9 in Reference [2].

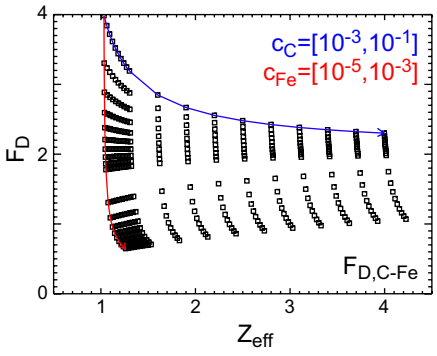

Figure 2: (Color online) Values of $\mathcal{F}_{D,C-Fe}$ limiting the maximum achievable density for various ranges of carbon and iron concentrations.

We now consider a semi-analytic model which includes the effects of island heating/cooling on the island growth, corresponding to being above/below the radiative power balance criteria described above. We use large aspect ratio cylindrical geometry r, θ with a conducting wall at minor radius $r = 1$

and model profiles[8]. Introduce a magnetic island with helical flux given by [6, 9] $\psi(r,\theta) = \psi_0(r) + \psi_1(r)cos(m\theta)$. The current density profile is given by $j = \nabla_\perp^2\psi + 2n/m + \delta j$, where δj is any additional modification of the current in the island. The helical flux satisfies

$$\nabla_\perp^2\psi_1 = \frac{dj}{d\psi_0}\psi_1 + \delta j_1, \tag{5}$$

and $\nabla_\perp^2\psi_k = \psi_k'' + \psi_k'/r - m^2\psi_k/r^2$. Saturation occurs when $\Delta'(w) = (\psi_1'(r_r) - \psi_1'(r_l))/\psi_1(r_s) = 0$, with the island edges r_l and r_r, and w the island width.

The perturbed current causes a change of Δ' given by the addition of $\Delta'_{\delta j}(w) = -w\delta j_1/\psi_1$. We solve for the island eigenfunction using the current profiles described in Reference [1] as being consistent with a tokamak at the density limit (the current profiles are from the familiar Furth-Rutherford-Selberg model [8]) with $r_0 = 0.548$, $\nu = 1.53$, $q(0) = 0.9$, $r_s = 0.729$. In Fig. 3 the calculated asymmetric island eigenfunction is shown.

Because of the island asymmetry, there is another destabilizing effect, not considered previously in disruption models. The term associated with asymmetry has been previously published in reference [11] in the context of island stabilization. In the island the current profile is flattened, producing a perturbed negative current (destabilizing) in the small minor radius side of the island and a positive current perturbation (stabilizing) in the large minor

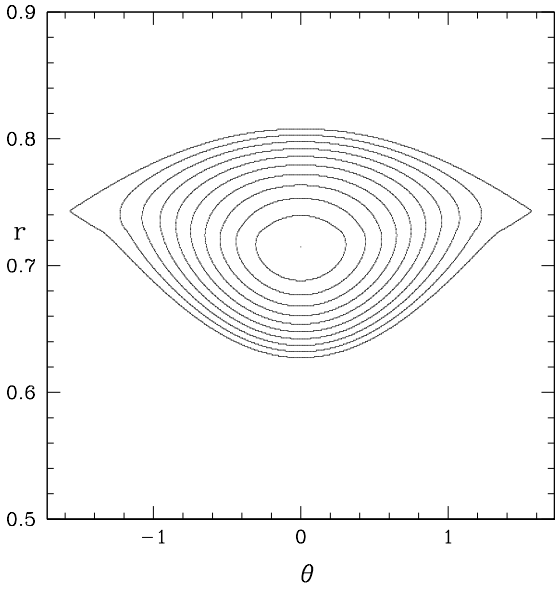

Figure 3: The saturated island flux surfaces.

radius side of the island. However, the island is flattened over only part of its width as was first shown in Reference [12]. The effect on Δ' is given by the addition of

$$\Delta'_A(w) = \frac{\int [j(r_x) - j(r)] cos(m\theta) d\theta dr}{\psi_1(r_s)} f_F, \tag{6}$$

with the subscript standing for asymmetry and f_F the fraction flattened and $j(r_x)$ is the current at the island X-point, with the integration being over the island. This is the first of the three important thermo-resistive effects.

For very small island width, perpendicular heat diffusion overwhelms the flattening and the normal equilibrium current profile is restored[12] re-

sulting in modifying $\Delta'_{\delta j}$ by the factor $w^2/(w^2 + w_F^2)$, with w_F given by $\sqrt{8}(\kappa_\perp/\kappa_\parallel)^{1/4}(Rr_s/ns)^{1/2}$, where $s = r_s q'/q$ is the local shear and $\kappa_\perp$ and $\kappa_\parallel$ are the cross field and parallel heat conduction constants. Since the current perturbation is caused by the perturbed temperature profile, the same consideration applies to Δ'_A. This effect, called the Fitzpatrick effect, is the second of the three important thermo-resistive effects.

A small change in the net power in the island leads to rapid growth of the island. Radiation loss can produce a negative temperature differential in the island interior, thereby increasing the resistivity, the current will then decrease and the island will grow. In the new larger island, the fixed temperature gradient will produce a new lower value of the temperature at the island O-point and an increase in Δ'. This will lead to a further increase in island size, and this process repeats. This concept was first discussed in Reference [13]. This effect, called the Rebut effect, is the third of three important thermo-resistive effects. The Rebut effect is modeled by imposing a fixed temperature gradient inside the island.

Combining the thermal non-linearities described above we get a new island evolution equation which describes island dynamics in accordance with the three-dimensional resistivity which results from the temperature pertur-

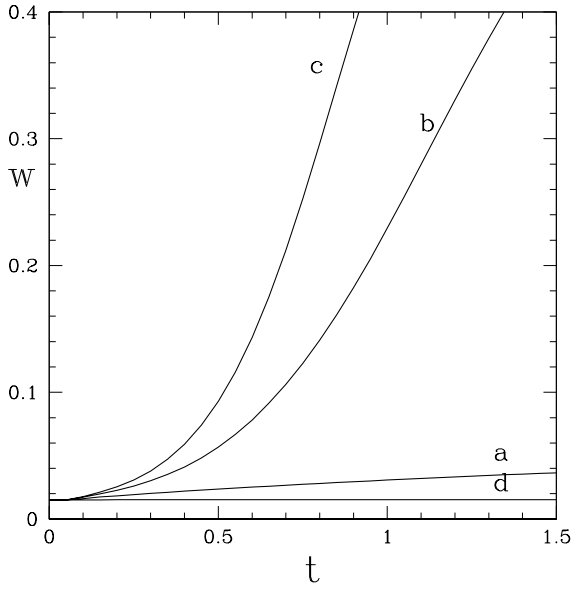

Figure 4: Growth of islands in an equilibrium with a fixed temperature gradient in the island. Shown is the island width vs. time (in units of local resistive time) for varying values of the fixed temperature gradient. At time $t = 0.2$ the imbalance produced an O-point temperature differential $(T_O - T_x)/T_x$ of a) 0, b) - 0.002, c) -0.003. In the case with heating, d) the temperature differential was 0.001.

bations due to the island.

$$\frac{dw}{dt} = r_s^2[\Delta'(w) + \Delta'_{\delta j}(w) + \Delta'_A(w)] \tag{7}$$

In Fig. 4 simulations of the island evolution made using Equation 7 are shown. The fixed temperature gradient in the island produced a lowered temperature at the island O-point of less than one percent at $w = 0.05$. Note that the temperature differentials necessary to produce rapid growth are small, not easily noticeable experimentally. This semi-analytic model is described in more detail in Reference [14].

We now turn to numerical simulations to corroborate the semi-analytic analysis. The simulations are developed by extension of the DEBS code[15] to identify the plasma regions inside magnetic islands and specify the balance of radiation and Ohmic heating in the island. DEBS is a nonlinear MHD initial value simulation code with cylindrical geometry, including radial finite difference representation, while the poloidal and axial directions are spectral.

The nonlinear MHD equations being advanced in the DEBS code are

$$\frac{\partial \vec{A}}{\partial t} = \vec{V} \times \vec{B} - \frac{\eta}{S_0}\vec{J} \quad (8)$$

$$\frac{\partial \vec{V}}{\partial t} = -\vec{V} \cdot \nabla \vec{V} + \frac{1}{\rho}\vec{J} \times \vec{B} - \frac{\beta_0}{2\rho}\nabla p + \frac{\nu}{\rho}\nabla^2 \vec{V} \quad (9)$$

$$\frac{\partial p}{\partial t} = -\nabla \cdot (p\vec{V}) - (\gamma - 1)p\nabla \cdot \vec{V} + \frac{1}{S_0}\nabla \cdot (\kappa_\perp \nabla_\perp T + \kappa_{||}\nabla_{||} T) \quad (10)$$

where $\nabla \times \vec{A} = \vec{B}$ and $\nabla \times \vec{B} = \vec{J}$. The key features that facilitate this study with DEBS are the implementation of anisotropic heat flux $q = \kappa_{||}\nabla_{||}T + \kappa_\perp \nabla_\perp T$ in combination with temperature dependent Spitzer resistivity $\eta(r, \theta, z) \sim T^{-3/2}$, which then responds to the structure of the temperature perturbation.

In the numerical simulations presented, the cylinder has an aspect ratio of $R/a = 2$, while the magnetic Reynolds number (the ratio of global resistive time to Alfven time) is held fixed at $S \equiv \tau_R/\tau_A = 10^6$ and the Prandtl number (the ratio of viscous diffusion to resistive diffusion) is held fixed at $P = \nu/\eta_0 = 0.1$. Radial resolution of 301 points, with 16 poloidal and toroidal modes is found sufficient for resolving the nonlinear mode.

A small equilibrium pressure with $\beta = P_0/B^2 = 0.005$ is included to drive the Ohmic physics through Spitzer resistivity. The pressure profile has a cubic polynomial structure allowing the edge and axis regions to have zero

gradients, while the edge pressure value P_{edge} is set small but finite to avoid negative pressure. The addition of pressure hardly alters the equilibrium fields and slightly decreases the linear growth rate of the mode, given the low β.

In extension of the DEBS code, within the simulation algorithm we calculate the helical flux to map island topology at each time step. With the helical flux, we determine which points in the computation are inside the island separatrix on the spatial grid, or the (r, θ, z) locations of the inverse Fourier transform of the simulation data in the spectral ($k_\theta = 2\pi m/r, k_z = -2\pi n/R$) representation. The helical flux is defined as:

$$\chi = mA_z(m, n) + k_z r A_\theta(m, n), \tag{11}$$

where (only) the $m/n = 2/1$ component of the perturbed fields is used to calculate the island structure. Once the island helical flux values are known, the separatrix value is used to determine the points on the grid that are inside the separatrix. We then map T_e to the island, imposing an internal island temperature as a function of island helical flux. This offers a simple method to capture the physics effects due to varying the net power inside the island.

Consistent with the semi-analytic analysis, we impose a linear dependence

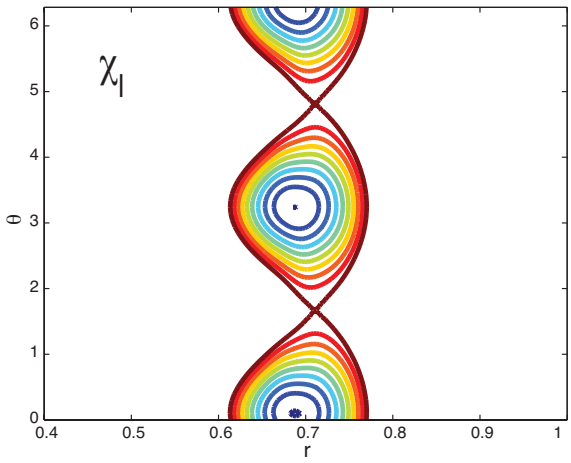

Figure 5: Contours of the helical flux inside the island.

on helical flux for the temperature inside the island. In all simulations the temperature dependence on helical flux inside the island is the only change in the simulation. Because β is low, force balance has little effect, and the physics dominating the response is through the 3D resistivity. The temperature at points outside the island is evolved via the usual anisotropic thermal conduction in the heat equation. Thus, imposing a constant temperature inside the island ($\nabla T = 0$) is comparable to having no imposed perturbation with strongly anisotropic heat conduction.

Contours of helical flux in the poloidal plane, indicating the asymmetric island $m/n = 2/1$ structure, with $\nabla T = -4$ are shown in Fig. 5. The inward bulging of the island is clear. The resonant surface $q = m/n$ shows a helical

deformation as evidenced by the displacement of the O-point radius inward relative to the X-points, consistent with the analytic model and experimental measurements of island structure[16]. This asymmetric structure is critical to the physics of the evolution.

With negative ∇T the island width grows rapidly to large size. The rate of growth increases rapidly with the gradient in temperature inside the island. In Fig. 6 is shown the full island width as a function of global resistive time for a series of cases with the balance of radiative cooling to Ohmic heating varied from net heating to net cooling, with the balanced case as reference. In the balanced case $\nabla T = 0$, the island grows to a saturated size that is comparable to the simulation without imposed inner island temperature dependence, where the anisotropic heat conduction effectively flattens the temperature.

Positive temperature gradient, or heated islands, cause saturation at a small island size. Fig. 6 shows that for $\nabla T = 1$ and 2, islands saturate well below the flattened $\nabla T = 0$ case. Even for very small values of negative temperature gradient (cooled islands) the islands grow rapidly. Note that the temperature perturbations are very small, in keeping with the semi-analytic model.

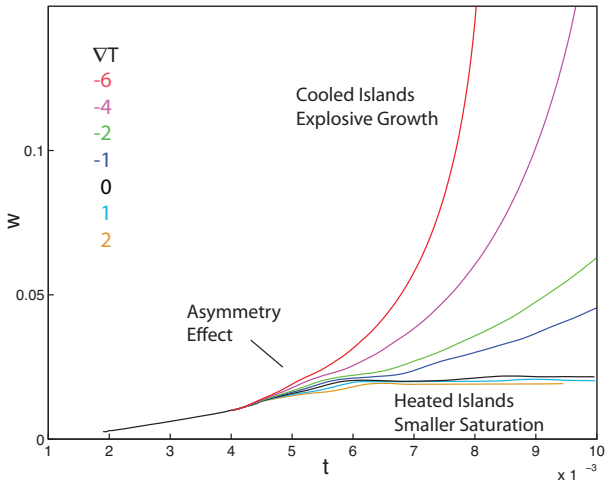

Figure 6: The island width as a function of time, in units of global resistive time, for a series of simulations with varying ∇T inside the island. The cooled islands exhibit rapid growth increasing with cooling, while the heated islands saturate at small size.

It has been show that 1) the island threshold criterion is nearly independent of Z_{eff} for a case with a dominant low Z impurity concentration, but with the radiated power dominated by a low concentration of high Z impurities, 2) that a simple model which includes all the important thermal non-linearities is robustly unstable with a sudden threshold for onset, and 3) that a fully nonlinear 3D MHD code can reproduce qualitatively the behaviors predicted by the analytic model. An important new term has been described for the Modified Rutherford Equation, referred to as the 'asymmetry term', which depends on the degree of island asymmetry. This term is necessary to reproduce the behavior of the full MHD model. With this term, the changes required in central island temperature to go from a small saturated island to instability is so small as to be nearly undetectable. In previous discussions of the thermal stability of islands [e.g., reference [17]], the idea of an island cooling term was dismissed because of the absence of a measurable depression in the measured temperature inside the island. A key point of this more complete model is that the drive for the islands does not require a large temperature depression because the asymmetry effect drives island growth at intermediate island widths. Given the simplicity and robustness of the concepts involved in this formulation, it seems likely that

there is general applicability of non-linearities driven by thermal structure in resistive magnetized plasma configurations (i.e, thermo-resistive effects) over a large range of parameters.

*This work was supported by the U.S. Department of Energy Grant under contract number DE-AC02-76CH03073 and Contract No. DE-SC0004125.

References

[1] D. A. Gates and L. Delgado-Aparicio, Phys. Rev. Lett. **108** (2012) 165004

[2] M. Greenwald, J.L. Terry, S.M. Wolfe S. Ejima, M.G. Bell, S.M. Kaye, G.H. Neilson, Nucl. Fusion **28** (1988) 2199.

[3] M. Greenwald, Plasma Phys. Control. Fusion **44** (2002) R27.

[4] D. A. Gates, L. Delgado-Aparicio, R. B. White, Nucl. Fusion **53** (2013) 063008.

[5] P. H. Rutherford, Phys. Fluids **16**, (1973) 1903.

[6] R. B. White, D. A. Monticello, M. N. Rosenbluth, and B. V. Waddell, Phys. Fluids **20**, 800 (1977).

[7] D. E. Post, R. V. Jensen, C. B. Tarter, W. H. Grassberger, W. A. Lokke, At. Data Nucl. Data Tables **20** (1977) 397.

[8] H. P. Furth, P. H. Rutherford and H. Selberg, Phys Fluids **16**, (1973) 1054.

[9] R. B. White, *The Theory of Toroidally Confined Plasmas, third edition*, Imperial College Press, pp. 191, (2014) 352.

[10] E. Fredrickson, M. Bell, R. V. Budny, and E. Synakowski, Phys of Plasmas **7**, (2000) 4112.

[11] E.Westerhof, A. Lazaros, E. Farshi, M.R. de Baar, M.F.M. de Bock, et al., Nucl. Fusion **47** (2007) 85-90

[12] R. Fitzpatrick, Phys Plasmas **2**, (1995) 825.

[13] P. H. Rebut and M. Hugon, Plasma Physics and Controlled Nuclear Fusion Research 1984 (Proc. 10th Int. Conf. London, 1984), Vol. 2, IAEA, Vienna, 197, (1985).

[14] R. B. White, D. A. Gates, D. P. Brennan, Phys. Plasmas **22** (2015) 022514

[15] D. D. Schnack, D.C. Barnes, Z. Mikic, J. Comp. Phys. **70**, (1987) 330.

[16] W. Suttrop, K. Buchl, J.C. Fuchs, M. Kaufmann, K. Lackner, et al., Nucl. Fusion, **37** (1997) 119.

[17] J. A. Wesson, R. D. Gill, M. Hugon, F. C. Schuller, J. A. Snipes, et al., Nucl. Fusion **29** (1989) 641.

PPPL PRINCETON PLASMA PHYSICS LABORATORY

Princeton Plasma Physics Laboratory
Office of Reports and Publications

Managed by
Princeton University

under contract with the
U.S. Department of Energy
(DE-AC02-09CH11466)

P.O. Box 451, Princeton, NJ 08543
Phone: 609-243-2245
Fax: 609-243-2751

E-mail: publications@pppl.gov

Website: http://www.pppl.gov